IOP Publishing Measurement Science and Technology
Meas. Sci. Technol. **29** (2018) 035107 (11pp) https://doi.org/10.1088/1361-6501/aa9fb8

Automated crack detection in conductive smart-concrete structures using a resistor mesh model

Austin Downey[1], Antonella D'Alessandro[2], Filippo Ubertini[2] and Simon Laflamme[1,3]

[1] Department of Civil, Construction, and Environmental Engineering, Iowa State University, Ames, IA, United States of America
[2] Department of Civil and Environmental Engineering, University of Perugia, Perugia, Italy
[3] Department of Electrical and Computer Engineering, Iowa State University, Ames, IA, United States of America

E-mail: adowney2@iastate.edu

Received 5 October 2017, revised 5 December 2017
Accepted for publication 7 December 2017
Published 15 February 2018

Abstract

Various nondestructive evaluation techniques are currently used to automatically detect and monitor cracks in concrete infrastructure. However, these methods often lack the scalability and cost-effectiveness over large geometries. A solution is the use of self-sensing carbon-doped cementitious materials. These self-sensing materials are capable of providing a measurable change in electrical output that can be related to their damage state. Previous work by the authors showed that a resistor mesh model could be used to track damage in structural components fabricated from electrically conductive concrete, where damage was located through the identification of high resistance value resistors in a resistor mesh model. In this work, an automated damage detection strategy that works through placing high value resistors into the previously developed resistor mesh model using a sequential Monte Carlo method is introduced. Here, high value resistors are used to mimic the internal condition of damaged cementitious specimens. The proposed automated damage detection method is experimentally validated using a $500 \times 500 \times 50$ mm^3 reinforced cement paste plate doped with multi-walled carbon nanotubes exposed to 100 identical impact tests. Results demonstrate that the proposed Monte Carlo method is capable of detecting and localizing the most prominent damage in a structure, demonstrating that automated damage detection in smart-concrete structures is a promising strategy for real-time structural health monitoring of civil infrastructure.

Keywords: self-sensing structural materials, smart concrete, smart structures, smart materials, structural health monitoring, Monte Carlo simulation, damage detection

(Some figures may appear in colour only in the online journal)

1. Introduction

Concrete is a widely used construction material for building civil infrastructure including highways, bridges, tunnels, and dams. The incorporation of appropriate monitoring capabilities into concrete structures would allow for real-time condition assessment, therefore reducing their overall maintenance expenditures while increasing safety. A key component to developing cost-effective condition-based maintenance programs for civil infrastructures is the development and application of efficient instrumentation and monitoring techniques. In particular, the automated detection of cracks in concrete can significantly contribute to the real-time monitoring of concrete infrastructure. While cracking is, to some extent, inherent to concrete structures, it can cause durability problems by exposing reinforcement bars to harsh environments

and can be an indicator of a loss in structural integrity. It follows that crack locations and conditions need to be accurately determined to yield the relevant structural assessments.

Several nondestructive evaluation (NDE) and testing methods exist for crack detection in concrete structures. Some of the most popular include ultrasonic methods [1, 2], x-ray tomography [3], ground penetrating radar [4], automated visual inspection [5], and acoustic emission-based [3, 6] testing methods. These methods, while well established, tend to require a significant amount of effort for setup and testing, making their use in automated long-term health monitoring deployments more difficult.

Another approach that has seen a high level of interest for monitoring of concrete structures, and other large infrastructures, is the use of dense sensor networks. These networks, often termed sensing skins, are thin electronic sheets that mimic the ability of biological skin to detect and localize damage over a structure's global area. Applied onto the surface of the structure, these sensing skins have demonstrated damage detection and localization capabilities, in particular for concrete substrates. Examples include a sensing sheet, under development by Tung *et al* [7], consisting of multiple full-bridge resistive strain gauges adhered to a polyimide substrate that is capable of detecting and localizing fatigue cracks in concrete test specimens. Hallaji *et al* [8] developed and deployed a thin layer of conductive copper paint applied to the surface of a concrete beam and demonstrated that damage in the concrete substrate results in local increases in the skin's electrical resistivity. These changes in electrical resistivity were mapped using electrical impedance tomography (EIT). Hou *et al* experimentally demonstrated the use of EIT for crack detection in a fiber reinforced cementitious composite under three-point bending [9]. While EIT has been shown to be capable of damage detection and localization in 2D applications under various configurations, including a carbon nanotube nanocomposite sensing skin [10], its application is complex because repeated measurements are required along with various applied currents to solve the tomography mapping inverse problem. Additionally, for cases with complex boundary conditions, the inverse mapping problem may be unsolvable.

Monitoring a structure's internal condition is also important as damage is not always detectable on a structure's surface. An example is grout failure, which can be caused by high levels of shear under seismic loading [11], where monitoring of internal conditions could be used in the engineering of retrofit solutions [12]. Other examples include the monitoring of thick slabs of reinforced concrete, such as load bearing walls or containment structures, where internal damage may not be evident on the surface [4]. A possible solution providing internal monitoring capabilities is the utilization of self-sensing concrete at key locations in the structure of interest [13]. These self-sensing cement-based materials are often termed smart-concrete or smart-cement-paste (depending on the presence of aggregates). Smart-concrete offers many benefits over embedded or external sensors, including similar mechanical properties to those of the structure being monitored, similar aesthetics, and the potential to provide monitoring over a structure's lifecycle as the sensors have essentially the same durability as the structure being monitored. Various methods for fabricating smart-concretes have been proposed. The doping of carbon-based fillers into traditional admixtures of cement-based materials has shown to be particularly promising [14]. Various carbon-based materials have been mixed with cementitious materials, including carbon fibers [6, 15], nano-carbon black [16] and, more recently, multi-walled carbon nanotubes (MWCNT) [17, 18]. MWCNTs offer great potential due to their excellent electrical and mechanical properties [19–21]. They have been employed in the fabrication of many strain sensing composite materials.

Research on self-sensing cement mixtures has demonstrated their strain-sensing capability for dynamic [18, 22] and transient [23, 24] loading cases. The static strain sensing capacities of smart-cement mixtures have shown to be more difficult due to their intrinsic signal drift in the time domain, theorized to be caused by material polarization [25, 26]. In addition to smart-cement-paste's strain-sensing capability, damage detection and localization has been performed for various forms of conductive cement composites in the form of data-driven damage detection, where damage is inferred from a change in electrical signal [6, 27–29]. However, the data-driven approaches for smart-cement mixtures lack the ability to localize damage within the structure. Localization of damage can be achieved through the incorporation of more electrodes and the assumption of a simple resistor-based model, as described for example in reference [29]. The introduction of more complex 2D resistor mesh models was recently proposed by the authors, whereby a damage could be localized in a smart-cement-paste structural component through the addition of damage detecting resistors to represent the cracks (discontinuities in current flow) [30]. While the resistor mesh model presented in [30] showed promise for detecting and localizing damage using a simple and computationally efficient method, it required that damaged resistors be manually added to the resistor mesh model in order to simulate damage. The automated placement of damaged resistors in the model was not addressed, a task that is needed to expand the usefulness of the propose resistor mesh model.

This work presents a process for the automated placement of resistors using a sequential Monte Carlo method using the recently proposed 2D resistor mesh model in an effort to improve the resistor mesh model's fit. This is done through defining a multi-objective optimization problem that seeks to reduce both the average and extreme error between the model's predictions and test results, using a multi-objective formulation borrowed from the fields of robust structural design [31] and optimal sensor placement [32]. It is hypothesized that damage can be located using the proposed resistor mesh model through increasing the fit between the model and the experimental data. Validation of the proposed method is conducted on a $500 \times 500 \times 50$ mm^3 cement-paste plate doped with MWCNT. Damage is introduced in the plate using 100 repeated impacts from a 3 kg hammer resulting in the formation of multiple cracks. Results show that the application of the sequential Monte Carlo method, when used to place damaged resistors in a resistor mesh model, is capable of tracking the most prominent damage in the plate.

2. Background

This section provides a brief review of the smart-cement-paste used in this research, including the measurement approach and the resistor mesh model designed for the smart-cement-paste application, as well as the adopted bi-optimization objective function.

2.1. Smart-cement-paste fabrication

The fabrication process and sensing principles of the smart-cement-paste used in this work were presented by D'Alessandro *et al* [17] and reviewed here for brevity. A cement matrix is doped with MWCNT to create a self-sensing cementitious material. This doping provides the cement-based composite with increased conductivity (reduced resistivity), the capability to detect damage in the form of changing resistance, and piezoresistive strain sensing properties. In the presented experiment, a single specimen was developed by adding 1% MWCNT (Arkema C100), with respect to the mass of cement, to the cementitious material. First the nanotubes were added to water along with a surfactant (a solution of a high molecular weight block copolymer with pigment affinic groups) and dispersed through sonication. Then, the nano-modified water suspension was mechanically mixed with cement thus obtaining the paste. For more details on the preparation procedure and the achieved quality of nanotube dispersion, the interested reader is referred to a previous work by the authors [17]. After mixing with cement, the smart-cement-paste was cast into a $500 \times 500 \times 50$ mm^3 mold with two steel reinforcement meshes. The meshes were made of 1.2 mm diameter steel wire arranged in a 60×60 mm^2 grid and stacked such that their wires and holes aligned. A total of 56 1.2 mm contacts were then inserted 40 mm into the uncured smart-cement-paste. Of these, only 36 were utilized for experimental testing. The effect of embedded contacts on the structural integrity of a structure is left to future work. For instance, one needs to investigate the appropriate contact depth that provides sufficient material bonding without reducing the integrity of the structure. These embedded contacts were placed evenly on an 80×80 mm^2 grid positioned about the center of the plate, while the unutilized contacts were placed along the perimeter between the utilized contacts. A schematic of the smart-cement-paste specimen is shown in figure 1. The specimen was allowed to cure for 28 days before testing began.

2.2. Biphasic measurement approach

The biphasic measurement approach recently proposed by the authors [26] allows for the temporal multi-channel monitoring of smart-cement materials through removing the polarization effect found in carbon-doped smart-cement-pastes [19, 22, 24, 26, 33]. The biphasic measurement approach functions by sourcing a periodic measure/discharge sensing current in the form of an alternating square wave from a power supply. In this work, a signal generator was used to produce a periodic square wave. This device was found to provide sufficient power due to the low current draw required. The periodic signal consists of a 'measure region' where DC voltage measurements are made

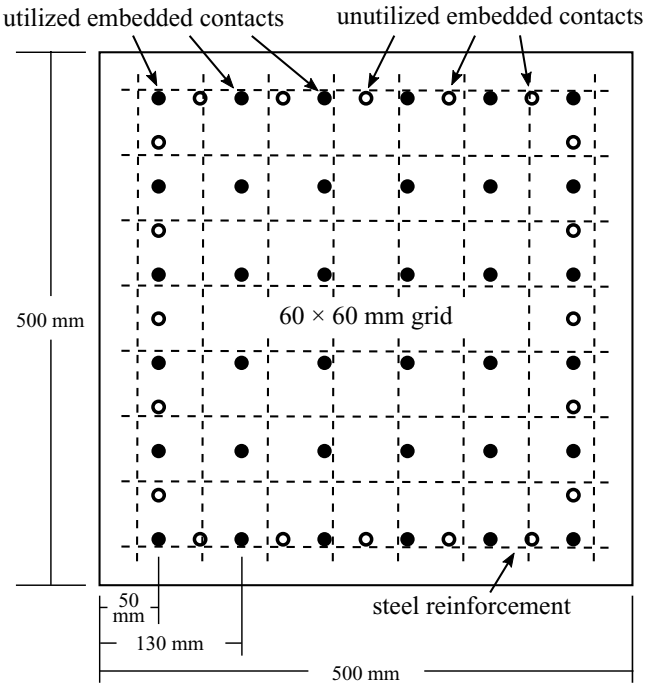

Figure 1. Key components and dimensions of the $500 \times 500 \times 50$ mm^3 smart-cement-paste specimen used in this study.

and a 'discharge region' where the material depolarization is obtained, as shown in figure 2(a). A DC voltage measurement is taken, termed sample point, after 80% of the measure region is completed. Due to the spatial distribution of the embedded contacts in this work, the voltage acquired at the sample point (figure 2(a)) is not used to calculate a resistance measurement. Instead, the DC voltage measurement, taken at the point corresponding to 80% of the measure region, is used as a direct input to the resistor mesh model.

Regardless of the embedded contacts' spatial distribution in the plate, the total resistance of the plate can be measured by monitoring the current flow through the entire plate. Figure 2(b) shows how this electrical resistance is also a function of the voltage (peak-to-peak) used in the periodic square wave, demonstrating that the material is not ohmic. A notable result in figure 2(b) is the reduction in the plate's resistance for an increase in the applied voltage. For instance, a 57.5% decrease in the plate's resistance is found over the tested range of 2–20 V_{pp}. In terms of designing specialized data acquisition equipment for the proposed resistor mesh model, the material's decrease in resistance associated with an increase in the applied voltage can be beneficial as it facilitates a larger voltage drop over the plate. Because of the higher voltage drop across the plate, the measured voltage at each contact will be higher and therefore can be easier to measure. This can help to reduce the complexity of measurement hardware required, a necessary improvement when developing long-term embedded data acquisition systems.

2.3. Resistor mesh model

The use of a resistor mesh model for damage detection, localization and quantification is the subject of another work by the

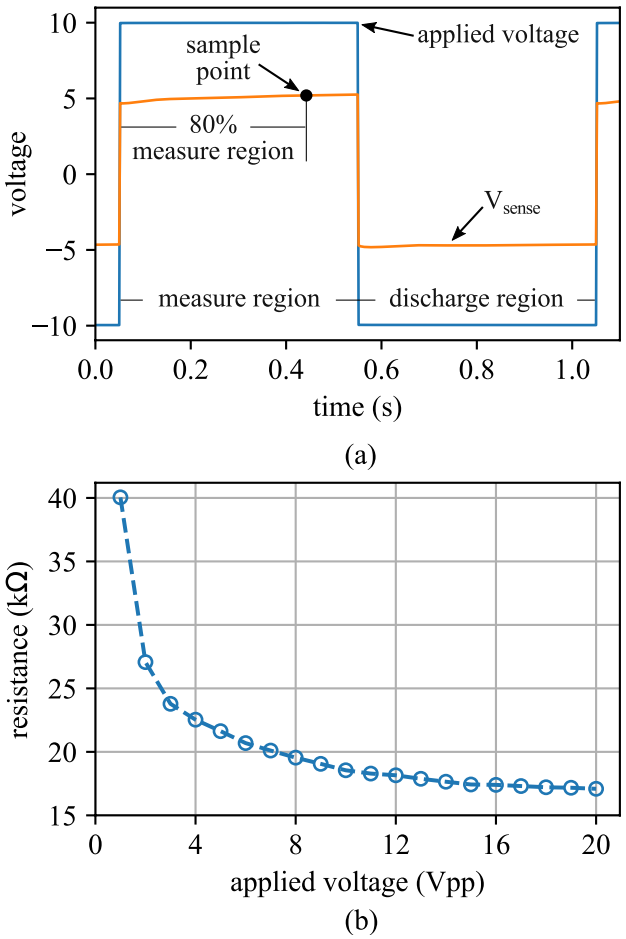

Figure 2. Measurement of the electrical output of smart-cement-paste: (a) using a biphasic DC signal at 1 Hz with 50% duty cycle showing the discharge and measure regions with the sample point annotated; (b) effect of changing biphasic peak to peak voltage levels on the measured resistance.

authors [30]. In brief, a 2D mesh is constructed to mimic the conductive specimen's geometry. This resistor mesh is constructed of resistors (intended to mimic the electrical response of the smart-cement-paste) and nodes (for voltage measurements at embedded contacts), allowing the resistor mesh to be solved using nodal analysis. The formulation of this nodal analysis problem only requires knowledge of the specimen's geometry and the applied voltage (V_{applied}) as model inputs. The assumption is made that damage present in the specimen will manifest itself as an increase in resistance in the plate. This increase in resistance will be measured as a change in voltage at an associated node. This reduction in conductivity is due to the property that cracks in the self-sensing material are considered to cause a reduction in conductivity as they are non-conductive when opened [18, 28, 29]. A resistor mesh model can then be constructed to mimic the internal condition of the specimens through the correct placement of damaged (high-value) resistors as required in order to minimize the error between the specimen's measured and the model's estimated nodal voltage values. For simplicity, the resistor model used in this work is solved in SPICE [34], an open-source analog electronic circuit simulator. For a known geometry, the resistor mesh model could be reconstructed as a set of linear equations to decrease its computation time. A decrease in computational complexity is a useful feature for the future development of embedded measurement systems that need to operate on limited computational resources.

Due to the nature of the impact loading cases in this study, the strain sensitivity of the smart-cement-paste is not considered. However, prior results showed that the resistor mesh model is capable of monitoring a smart-cement-paste's strain condition through adjusting a resistor's values based on its strain state, both before and after a failure occurs [30].

2.4. Bi-optimization objective function

The effective placement of resistors requires the definition of an optimization objective function. The simplest form of an objective function would be a spatially averaged absolute difference of the error between the measured voltage at each node and the model's estimated voltage at the same node. While simple, this approach may result in a solution with a few single points of high disagreement, therefore resulting in a solution that does not truly represent the condition of the plate being monitored. A solution to this problem would be to only optimize the points of highest disagreement between the plate's measured state and the model. However, this would introduce other issues including longer computational time and an increased probability of converging to a local minimum. Therefore, a bi-optimization objective function that reduces both the average and point-of-highest error between the plate's measured state and the model is needed.

For the purpose of reducing the mean error between the plate's measured state and the model's representation, an optimization problem based on minimizing the mean absolute error (MAE) is utilized. The use of MAE for validation provides a simple, yet effective representation of how well a given model represents the structure. Additionally, to reduce the severity of points of highest disagreement, a second optimization problem based on minimizing the maximum difference between any contact's sensed voltage and model's estimated voltage is introduced, defined as β. The bi-objective optimization problem for selecting a vector, $\mathbf{R}$, of resistance values for the resistor mesh model can be formulated as

$$\begin{aligned} \underset{\mathbf{R}}{\text{minimize}} \quad & f(\mathbf{R}) = \big(\text{MAE}(\mathbf{R}), \beta(\mathbf{R})\big) \\ \text{subject to} \quad & \mathbf{R} = [r_1 ... r_m]^{\mathrm{T}} \in \mathbb{R} \end{aligned} \tag{1}$$

where $\mathbf{R}$ is a unique vector consisting of m resistor values taken from the resistor set $\mathbb{R}$ that consists of all the potential resistor values under consideration.

The multi-optimization problem presented here can be combined with solutions that lie close to the Pareto frontier to form a single objective optimization function. While various methods have been proposed for finding the various solutions that lie on or near the Pareto frontier, a straightforward scalarization approach is used here. Formulated as a linear combination method, the selected approach seeks to find the minimum of a weighted combination of the two objective functions, MAE($\mathbf{R}$) and $\beta(\mathbf{R})$. This approach allows for the trade-offs between the two objectives to be adjusted through the scalarization

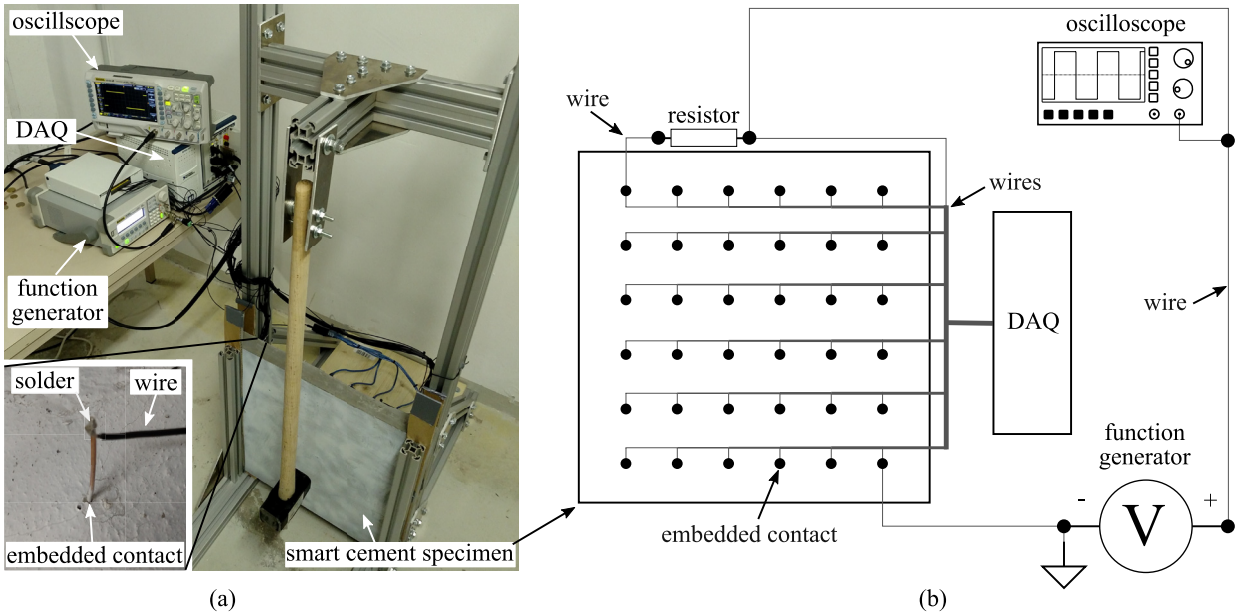

Figure 3. Experimental test setup showing the (a) key components used in the impact testing of the smart-cement-paste plate with an embedded copper contact shown in the inset; (b) electrical test schematic showing the connection of the data acquisition system (DAQ) to the test specimen with key system components annotated.

parameter (α), thereby increasing the usability of the optimization function. The single objective problem for optimizing the selection of a resistor set $\mathbf{R}$ can be formulated as

$$\begin{aligned} &\underset{\mathbf{R}}{\text{minimize}} && \text{fit} = (1-\alpha)\frac{\text{MAE}(\mathbf{R})}{\text{MAE}'} + \alpha\frac{\beta(\mathbf{R})}{\beta'} \\ &\text{subject to} && \mathbf{R} = [r_1 \ldots r_m]^{\mathrm{T}} \in \mathbb{R} \\ &0 \leqslant \alpha \leqslant 1 \end{aligned} \tag{2}$$

where MAE' and β' are factors used for normalizing $\text{MAE}(\mathbf{R})$ and $\beta(\mathbf{R})$. These factors are evaluated by solving the resistor mesh model for an initial resistor set $\mathbf{R}_{\text{initial}}$, that minimizes the current draw error and then solving for the normalizing factors with $\text{MAE}' = \text{MAE}(\mathbf{R}_{\text{initial}})$ and $\beta' = \beta(\mathbf{R}_{\text{initial}})$.

As expressed in equation (2), the bi-optimization function can be converted to a single optimization problem that seeks to minimize only the MAE or β value by setting $\alpha = 0$ or 1, respectively. The selection of an appropriate α value is based on the capability of the resistor mesh model to accurately represent the plate's condition and such a selection can be achieved through numerical investigation.

3. Methodology

This section introduces the methodology used for investigating the automated placement of resistors in a resistor mesh model, including the test setup, the selected model arrangement, and the sequential Monte Carlo algorithm.

3.1. Test setup

Experimental results for a cracked plate were obtained through the repetitive impact loading of a smart-cement-paste plate, as shown in figure 3(a). Here, a $500 \times 500 \times 50$ mm^3 plate with 36 embedded contacts was mounted vertically in an extruded aluminum frame. A 3 kg hammer, also mounted on the aluminum frame, was used to provide 100 near identical impacts to the center of the plate. For each impact the hammer handle was rotated back 20° from the vertical and released to induce a single impact into the plate. At its fully displaced position, the hammer head was raised 5 cm and stored an estimated 1.5 J of energy. The biphasic signal was sourced from a function generator (Rigol DG1022a) as a 20 V_{pp} square wave with a frequency of 1 Hz and a 50% duty cycle. The applied voltage of 20 V_{pp} is constant throughout the test (i.e. the test can be considered as voltage controlled). The contact resistance between the copper contact and the smart cementitious material has been shown to be high [35]. However, as the contact resistance only affects the current carrying contacts [36], this aspect is only relevant at the current input (top-left contact in figure 3(b)) and output (bottom-right contact in figure 3(b)) copper contacts. Other than the voltage sample taken at the current input and output contacts, the voltage sample taken at the copper contacts is not affected by the contact resistance. Voltage samples were taken using one of two analog input modules (PXIe-4302 and PXIe-6361 mounted in a National Instruments PXIe-1071 chassis) at each of the plate's embedded contacts. Wires were soldered to the embedded copper contacts, as shown in the insert of figure 3(a), and connected to the analog input modules. The 1 Hz biphasic signal dictates that measurements were made at 1 sample per second (S/s). Therefore, a DC voltage measurement is taken once per second at the point where 80% of the measure region is completed and is used as an input to the resistor mesh model. An oscilloscope (Rigol DS-1054), acquiring the biphasic signal, was used during testing for validation purposes only. The schematic of the measurement system is presented in figure 3(b) with the key components annotated.

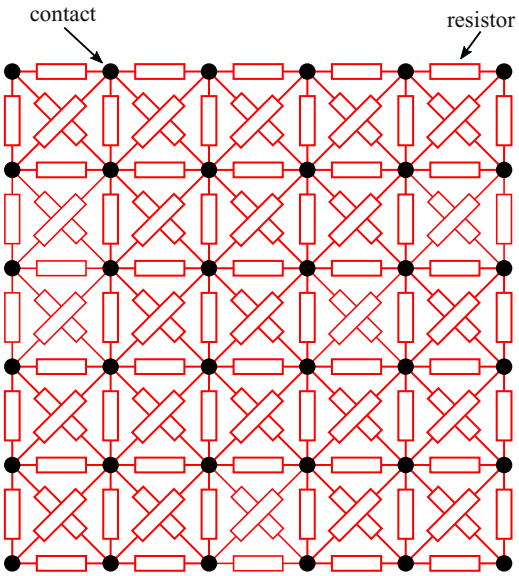

Figure 4. The resistor mesh model used for the electrical modeling of the plate.

3.2. Resistor mesh model

The configuration of the plate's resistor mesh model is presented in figure 4. A resistor mesh model of 110 resistors was selected to connect the 36 voltage nodes as it reproduced the majority of possible conductive paths through the plate. The diagonal resistors are independent of each other and do not form a conductive path where they cross each other due to the lack of a contact point. Simpler resistor mesh models were investigated and were found to provide comparable results. These included models without the diagonal resistors, or with subsets of the diagonal resistors. However, the reduction in the number of resistors reduces the resistor density, resulting in a lower damage localization resolution. In addition, a 160 resistor mesh model that added a node at the center of the diagonal resistors was investigated. The addition of model nodes without corresponding experimental nodal data caused the sequential Monte Carlo simulation to converge to a local minimum solution rather than to a truly global minimum solution. Therefore, it was decided that the mesh model with 110 resistors provided the best results for the current study.

3.3. Sequential Monte Carlo algorithm

The sequential Monte Carlo algorithm presented here is a variation of a typical Monte Carlo approach that uses repeated random sampling to obtain a numerical estimation of a resistor set that is capable of modeling crack damage in the conductive smart-cement-paste plate. The algorithm is diagrammed in figure 5. First, an initial constant value (parent) for $\mathbf{R}$, termed $\mathbf{R}_{\text{initial}}$, is obtained by minimizing the error between the model's total current flow and the healthy plate's total current flow while considering the contact resistance present at the current carrying contacts [35]. This minimization is done using a simple gradient descent algorithm. Once $\mathbf{R}_{\text{initial}}$ is obtained, a

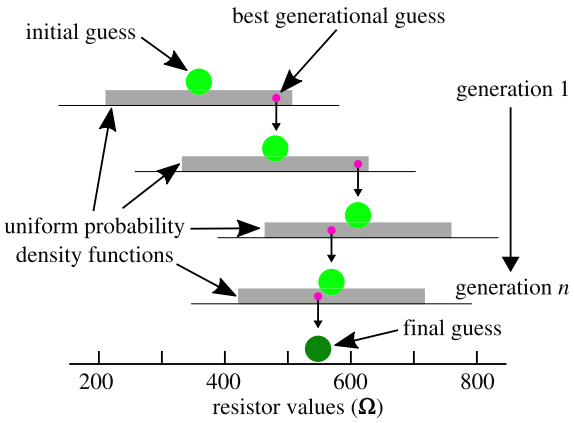

Figure 5. Visualization of the sequential Monte Carlo process used in this work.

population set consisting of a number of unique values of $\mathbf{R}$ is generated by sampling new resistor values (r) for the r values in $\mathbf{R}_{\text{initial}}$. A particular resistance value for a new generation is taken from a uniform distribution that is centered about the initial guess over a distribution of resistance values where the width of this distribution is termed R_{range}. The population set consisting of the unique $\mathbf{R}$s can then be solved and its error calculated using equation (2). The $\mathbf{R}$ vector that produces the lowest error is selected as the new parent and the population for the next generation is then mutated from this parent. This process is repeated for a set number of generations, after which the final $\mathbf{R}$ vector is the numerical estimation of a resistor set that best reproduces the spatial resistance distribution in the conductive smart-cement-paste plate. Pseudo code for the sequential Monte Carlo algorithm is presented in algorithm 1 with the SPICE models solved in parallel.

Algorithm 1. Sequential Monte Carlo algorithm used in this work.

```
calculate R_initial
R = R_initial
for generation count do
    parfor population count do
        R_i = Monte_Carlo(R)
        fit_i = SPICE(R_i)
    end parfor
    best = index(minimum(fit))
    R = R_best
end for
R_final = R
```

The application of the sequential Monte Carlo algorithm requires the tuning of certain parameters and, in particular, of R_{range}, α, population size and the number of sequential generations needed to achieve a numerical estimation of sufficient quality. In this work, the selection of parameters was done during a preliminary investigation by first making educated guesses about the values for R_{range} and α. Then, the population number and generational count were investigated over a wide range of possible values for both the healthy and damaged state (100 hammer impacts), with values taken in a way to optimize the final fitting results without incurring extensive computational costs. The selected population size

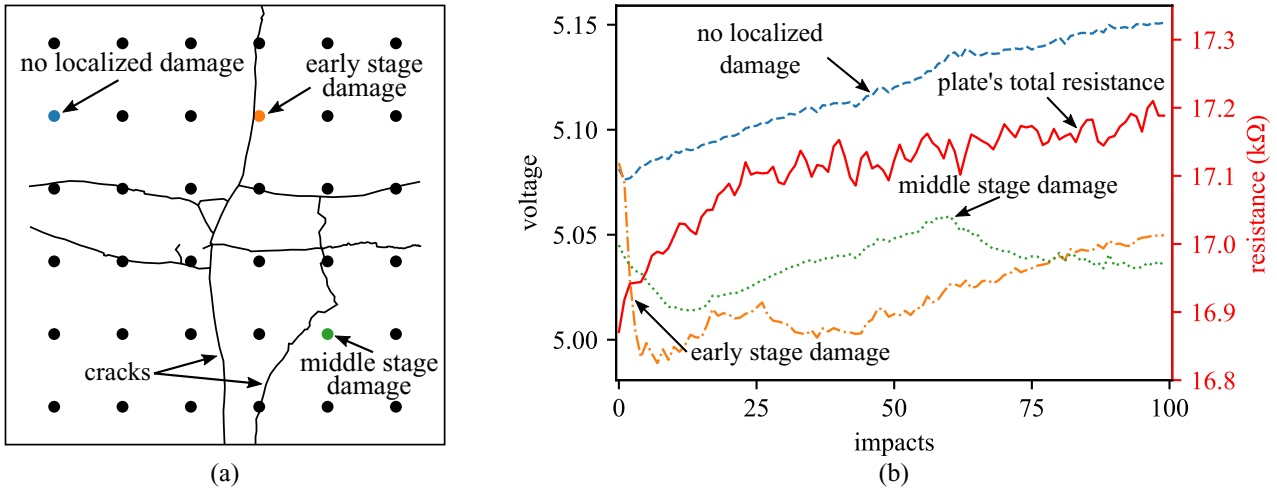

Figure 6. A purely data-driven damage detection analysis (no resistor mesh model) for the test plate showing (a) damage and the location of inspection points, and (b) the change in the plate's total resistance and the change in voltage data taken at the three inspection points of interest, selected to show damage forming during different portions of the test.

and generation number were then used to recursively investigate the effects of R_{range} and α on the final solution using a series of repeated algorithm runs at each inspection point.

4. Results

This section reports the results from the experimental testing, including a parametric study on the sequential Monte Carlo algorithm.

4.1. Data-driven damage detection

First, a purely data-driven approach to damage detection using the plate's total resistance and the voltage monitored at the embedded contacts is investigated. These results are presented in figure 6. The annotated cracks for the plate's fully damaged state, after 100 hammer impacts, are illustrated in figure 6(a). The simplest form of damage detection in smart-cement-paste is achieved through monitoring the plate's total resistance value. This total resistance value can be obtained through a standard two-probe measurement that accounts for the plate's total resistance, including its contact resistance. This method is also applicable to the specimen under consideration through tracking the change in resistance (solid red line in figure 6(b)). It can be observed that the majority of the damage occurred during the first 25 hammer impacts. After, the damage continues to increase with each subsequent impact, but at a lower rate. While useful in assessing the plate's global health, monitoring the plate's resistance value does not provide any useful measure of the localization of damage within the plate.

A qualitative estimation for the localization of damage within the plate can be achieved through the investigation of temporal voltage samples at the embedded contacts. In figure 6(b) the dashed blue line is the voltage data for a contact in the upper left of the plate, a region that experienced no visible cracking during testing. The mostly linear increase in the measured voltage is attributed to the sum of the voltage drops that must equal the applied voltage. Thus, if the formation of a crack causes a change in resistance in one portion of the plate, the entire plate must find a new equilibrium. In contrast, voltage samples reported by the orange dot-dashed line in figure 6(b) exhibits damage that is formed near an embedded contact during the first few hammer impacts. Lastly, the dotted green line in figure 6(b) shows a change in its voltage data around hammer impact 60, which discontinuity in voltage is presumed to be related to the neighboring crack seen in figure 6(a). Growth in this crack was visually observed during testing and recorded by a high-resolution digital camera. While showing some promise for localization of damage, these temporal variations in the voltage samples do not provide a quantitative value for damage.

4.2. Parameter study

The use of the Monte Carlo algorithm, presented in section 3.3, requires the tuning of parameters (population, generations, R_{range} and α) before the algorithm can be used for damage detection and localization. Figure 7 presents the results for the population and generation study for both the healthy (figure 7(a)) and damaged (figure 7(b)) cases with $R_{\text{range}} = 100\ \Omega$ and $\alpha = 0.5$. In total, 100 population/generation combinations were inspected for each plate condition. As expected, the final fit value for both cases improves as both the population and generation size increase. The improvement in fit per added population or generation is greatest at the early stages of increasing the population or generation count used in the Monte Carlo simulation. The damaged cases, shown in figure 7(b), consistently demonstrated a slightly worse final fit for any given population/generation point. This is due to the damaged plate requiring a more diverse resistor mesh model to reproduce the plate's condition. On average, for any given generation/population the final fit for the damaged condition was 43.4% higher than that of the healthy condition. To provide an accurate representation of the Monte Carlo algorithm for placing resistors into the resistor mesh network, while optimizing the number of SPICE simulations required,

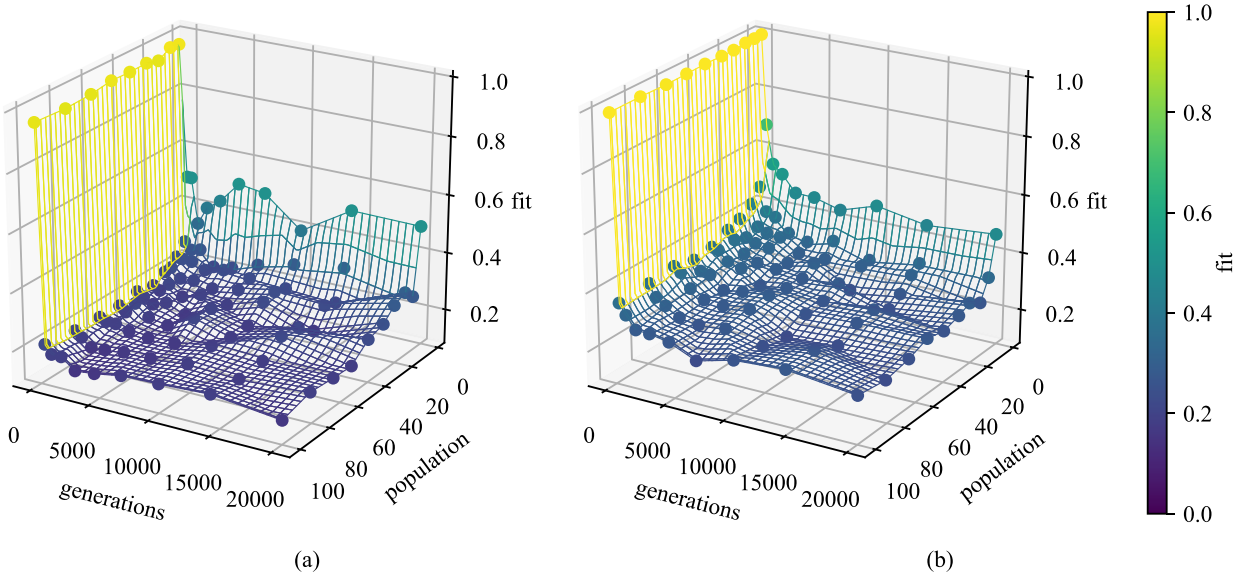

Figure 7. Sequential Monte Carlo fit results, as defined in equation (2), as a function of population size and number of generations for the smart-cement-paste specimen in (a) healthy and (b) damaged condition.

a population size of 50 with 20 000 generations is used throughout the remainder of this work. This results in each simulation run requiring 1 million SPICE models be solved, a task that is completed in 5 h on a 12-core computer node running at 2.2 GHz.

Following the determination of the population and generation counts, the values for R_{range} and α are investigated and presented in figure 8. First, the effect of changing R_{range} is investigated for the damaged case using a population of 50, 20 000 generations and $\alpha = 0.5$, yielding the results presented in figure 8(a). Here, 50 R_{range} values ranging from 1 to 1000 Ω are investigated, whereby each inspection point is repeated 3 times for a total of 150 runs. As expected, the lowest value investigated (1 Ω) results in a poor final fit as the available range for the variation in the resistors is limited. As the range is increased, the capability of the Monte Carlo algorithm to obtain a better final fit value is increased. After a certain point, corresponding to $R_{\text{range}} \approx 200$ in this case, the potential range becomes too large and the capability of the algorithm to consistently obtain low final fit values is negatively affected. This is attributed to the Monte Carlo simulations converging to local minima. A general representation of the effect of a changing R_{range} on the final fit is presented in figure 8(a) as a 4th order polynomial that ignores the first data point. Based on these results, a range of $R_{\text{range}} = 100$ is selected and used throughout the remainder of this work.

Next, the effect of varying α on the fitting parameters, MAE and β, is investigated, with results shown in figure 8(b) with the best fit lines for each parameter taken as 4th order polynomials. Here, 30 inspection points ranging from $\alpha = 0$ to $\alpha = 1$ are considered, with 3 runs per inspection point, resulting in a total of 90 runs. Results show that the proposed objective function is capable of developing an **R** vector that can effectively minimize both the mean error (MAE) and the point of greatest disagreement (β). For the damaged plate considered in this example, with the MAE and β parameters taken

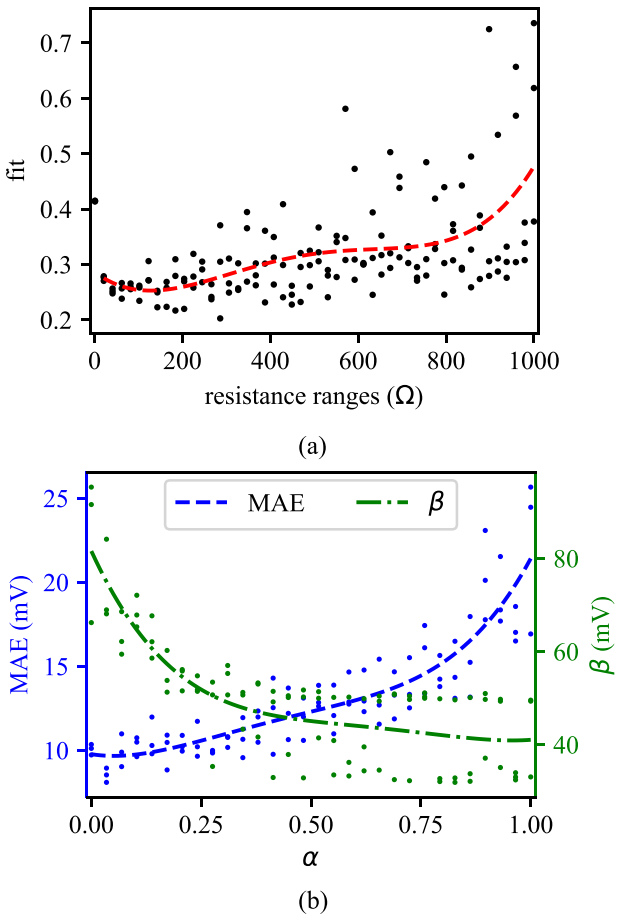

Figure 8. Investigation of the (a) R_{range} value on the final fit results, and (b) changing α parameter on the MAE and β results.

of equal importance, results indicated that $\alpha = 0.5$ provides an acceptable level of optimization for **R**. In addition, when compared with a single objective function based purely on the

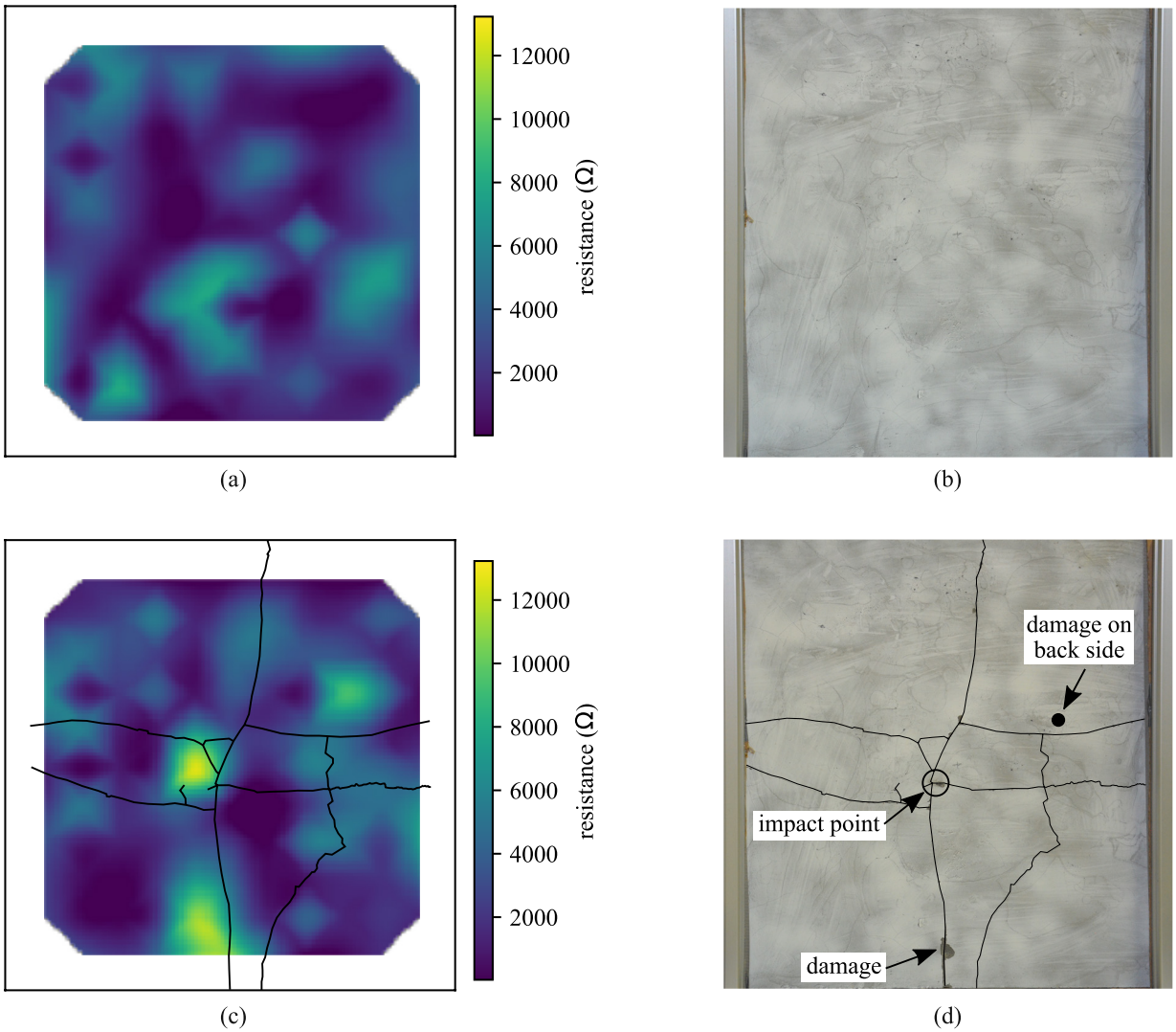

Figure 9. Final damage detection results showing the (a) spatial distribution of high-value resistors for the healthy state; (b) healthy test specimen; (c) spatial distribution of high-value resistors for the damaged state with crack distribution overlaid to show the relationship between damage and points of high resistance; (d) damaged (100 impacts) test specimen.

MAE (i.e. $\alpha = 0$), the selected value of $\alpha = 0.5$ provides a 45% improvement in the β value, while only increasing the MAE value by 19%. The best value of α is case-specific, but 0.5 is selected based on the presented results.

4.3. Damage localization

The capability of the sequential Monte Carlo algorithm to locate damage present in a concrete plate is illustrated in figures 9 and 10 where figure 9 presents the resistor mesh results and provides a picture of the plate's condition, while figure 10 presents the change in resistance between the healthy and fully damaged conditions (i.e. figure 9(c) minus figure 9(a)). The final fit obtained for the healthy condition was 0.16 compared to 0.26 for the damaged condition. The optimized resistors for the healthy condition were found to be relatively constant, with a maximum value of 7500 Ω. In the case of the healthy plate, the resistor mesh model is assumed to track deviations in the resistive continuity and, therefore, the dispersion of the MWCNT within the plate. A more detailed study is required to investigate the use of a resistor mesh model for validating the quality of dispersion of conductive inclusions within a plate, as well as the local moisture content, and is left to future work.

For the damaged case, the sequential Monte Carlo algorithm is capable of placing damaged resistors at the points where damage is more significant. This is attributed to the sequential Monte Carlo algorithm focusing on placing the most damaged resistors first, therefore making detection of smaller damages more difficult. Additionally, the sequential Monte Carlo algorithm quantifies damage in a relative manner, as it seeks to compare the healthy to the damaged locations on the plate. The resistor mesh model, with the automated placement of resistors, was capable of detecting the three prominent damage points on the plate. These included the hammer impact point in the center of the plate, a damage point on the bottom-center (front and back) of the plate that experienced spalling (loss of material) during the first few hammer impacts, and above the center-right where a piece of concrete on the back of the plate was lost around the 80th hammer hit. The damage on the back side of the plate measured approximately $25 \times 12 \times 10$ mm^3

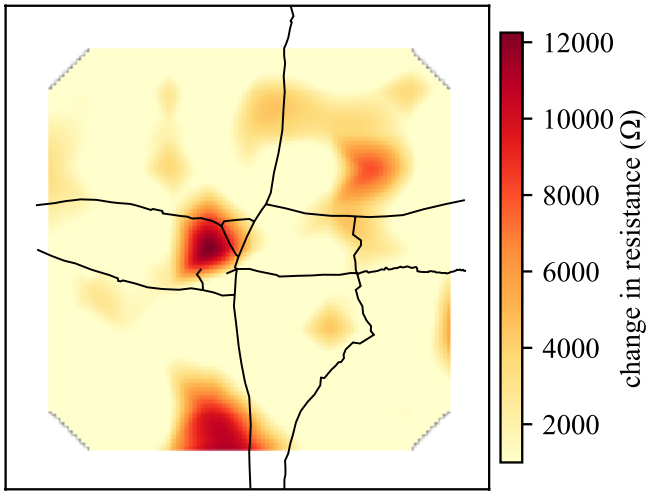

Figure 10. Final results for the plate showing the relative change in resistance for the damaged condition when compared to the healthy condition.

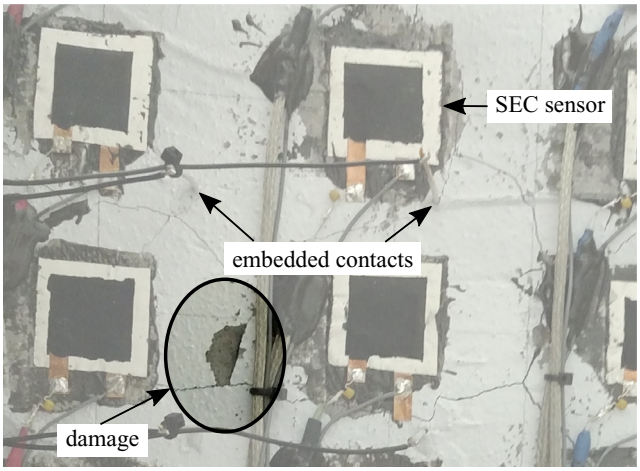

Figure 11. Concentrated spalling damage on the back of the plate as viewed from the back, additional sensors (SEC sensors) present in the figure are not discussed in this work.

(height × width × depth) and is detailed in figure 11. The large white/black squares present in this figure are novel large area sensors, termed the soft elastomeric capacitors and denoted as 'SEC sensor' in figure 11. These sensors were tested jointly and are out-of-the-scope of this work.

Results demonstrate that the resistor mesh model is capable of detecting damage, irrespective of its depth within the plate: a feature deemed useful when inspecting concrete structures where only one side of a structure is accessible. Increasing the damage detection and localization accuracy of the proposed resistor mesh model will require further study and development of more advanced algorithms for placing damaged resistors and further investigation of optimum contact layout and density. While in the current electrode configuration the resistor mesh model is not capable of determining the depth of prospective damage, this could be possible through the use of a 3D resistor mesh model. This more complicated modeling problem is left to future work.

5. Conclusion

A 2D resistor mesh model was shown to be capable of detecting and localizing damage in a conductive smart-concrete plate through the automatic placement of resistors using a sequential Monte Carlo algorithm. A resistor mesh model functions through developing an electrical model of the smart-concrete structural component that consists of a network of resistors, where damage is introduced into the resistor mesh network as a resistor of higher resistance value. This work introduced the automated placement of damaged resistors using a simple sequential Monte Carlo algorithm. This algorithm works through mutating an initial best guess for all the resistors, set through minimizing the difference between experimental and model electrical responses, by randomly selecting new values of resistors from a uniform probability density function of a certain resistance range. This step is repeated multiple times to form a population of new guesses, after which the best performing member of the population is selected as the new parent resistor set, which is then mutated in the following generation. Once a sufficient number of generations have been computed, the final resistor set can be used to spatially map the high resistance areas of the plate. It then follows that areas of high resistance can be correlated to prominent damages, while locations of low resistance can be considered as relatively undamaged.

Results demonstrated that the proposed approach is capable of damage detection within structural elements made of smart concrete. The automated placement of damaged resistors has the potential of enabling real-time detection, localization and quantification of crack-type damage using simple and inexpensive electrical hardware. Future work includes the development of search algorithms that provide better fitting results and reduce the required computational time. Additional areas of interest include the expansion of the proposed resistor mesh model into the third dimension and the quantification of the effects of reinforcement bars in full-scale reinforced concrete structures.

Acknowledgments

The support of the Italian Ministry of Education, University and Research (MIUR) through the funded Project of Relevant National Interest (PRIN) entitled 'SMART-BRICK: Novel strain-sensing nano-composite clay brick enabling self-monitoring masonry structures' (protocol no. 2015MS5L27) is gratefully acknowledged. This work is also partly supported by the National Science Foundation, Grant No. 1069283, which supports the activities of the Integrative Graduate Education and Research Traineeship (IGERT) in Wind Energy Science, Engineering and Policy (WESEP) at Iowa State University. Their support is gratefully acknowledged.

ORCID iDs

Austin Downey https://orcid.org/0000-0002-5524-2416
Antonella D'Alessandro https://orcid.org/0000-0003-2928-1961
Filippo Ubertini https://orcid.org/0000-0002-5044-8482
Simon Laflamme https://orcid.org/0000-0002-0601-9664

References

[1] Clayton D A, Smith C M, Ferraro C C Dr, Nelson J, Khazanovich L Dr, Hoegh K Dr, Chintakunta S and Popovics J Dr 2013 Evaluation of ultrasonic techniques on concrete structures *Technical Report* Oak Ridge National Laboratory (ORNL)

[2] Breysse D 2012 Nondestructive evaluation of concrete strength: an historical review and a new perspective by combining NDT methods *Constr. Build. Mater.* **33** 139–63

[3] Suzuki T, Ogata H, Takada R, Aoki M and Ohtsu M 2010 Use of acoustic emission and x-ray computed tomography for damage evaluation of freeze-thawed concrete *Constr. Build. Mater.* **24** 2347–52

[4] Eisenmann D, Margetan F J, Koester L and Clayton D 2016 *Inspection of a Large Concrete Block Containing Embedded Defects Using Ground Penetrating Radar* (Melville, NY: AIP Publishing LLC) (https://doi.org/10.1063/1.4940460)

[5] Prasanna P, Dana K J, Gucunski N, Basily B B, La H M, Lim R S and Parvardeh H 2016 Automated crack detection on concrete bridges *IEEE Trans. Autom. Sci. Eng.* **13** 591–9

[6] Chen B and Liu J 2008 Damage in carbon fiber-reinforced concrete, monitored by both electrical resistance measurement and acoustic emission analysis *Constr. Build. Mater.* **22** 2196–201

[7] Tung S-T and Glisic B 2016 Sensing sheet: the response of full-bridge strain sensors to thermal variations for detecting and characterizing cracks *Meas. Sci. Technol.* **27** 124010

[8] Hallaji M, Seppänen A and Pour-Ghaz M 2014 Electrical impedance tomography-based sensing skin for quantitative imaging of damage in concrete *Smart Mater. Struct.* **23** 085001

[9] Hou T-C and Lynch J P 2008 Electrical impedance tomographic methods for sensing strain fields and crack damage in cementitious structures *J. Intell. Mater. Syst. Struct.* **20** 1363–79

[10] Loh K J, Hou T-C, Lynch J P and Kotov N A 2009 Carbon nanotube sensing skins for spatial strain and impact damage identification *J. Nondestruct. Eval.* **28** 9–25

[11] Haber Z B, Saiidi M S and Sanders D H 2014 Seismic performance of precast columns with mechanically spliced column-footing connections *ACI Struct. J.* **111** 639–50

[12] Priestley M and Seible F 1995 Design of seismic retrofit measures for concrete and masonry structures *Constr. Build. Mater.* **9** 365–77

[13] Han B, Ding S and Yu X 2015 Intrinsic self-sensing concrete and structures: a review *Measurement* **59** 110–28

[14] Han B, Sun S, Ding S, Zhang L, Yu X and Ou J 2015 Review of nanocarbon-engineered multifunctional cementitious composites *Composites* A **70** 69–81

[15] Wen S and Chung D 2006 Model of piezoresistivity in carbon fiber cement *Cement Concr. Res.* **36** 1879–85

[16] Li H, Xiao H G and Ou J P 2006 Effect of compressive strain on electrical resistivity of carbon black-filled cement-based composites *Cement Concr. Compos.* **28** 824–8

[17] D'Alessandro A, Rallini M, Ubertini F, Materazzi A L and Kenny J M 2016 Investigations on scalable fabrication procedures for self-sensing carbon nanotube cement-matrix composites for SHM applications *Cement Concr. Compos.* **65** 200–13

[18] Azhari F and Banthia N 2012 Cement-based sensors with carbon fibers and carbon nanotubes for piezoresistive sensing *Cement Concr. Compos.* **34** 866–73

[19] Han B, Zhang K, Yu X, Kwon E and Ou J 2012 Electrical characteristics and pressure-sensitive response measurements of carboxyl MWNT/cement composites *Cement Concr. Compos.* **34** 794–800

[20] Gdoutos E E, Konsta-Gdoutos M S, Danoglidis P A and Shah S P 2016 Advanced cement based nanocomposites reinforced with MWCNTs and CNFs *Frontiers Struct. Civ. Eng.* **10** 142–9

[21] D'Alessandro A, Ubertini F, Materazzi A L, Laflamme S and Porfiri M 2014 Electromechanical modelling of a new class of nanocomposite cement-based sensors for structural health monitoring *Struct. Health Monit.* **14** 137–47

[22] Ubertini F, Materazzi A L, D'Alessandro A and Laflamme S 2014 Natural frequencies identification of a reinforced concrete beam using carbon nanotube cement-based sensors *Eng. Struct.* **60** 265–75

[23] Han B, Yu X and Kwon E 2009 A self-sensing carbon nanotube/cement composite for traffic monitoring *Nanotechnology* **20** 445501

[24] Monteiro A, Loredo A, Costa P, Oeser M and Cachim P 2017 A pressure-sensitive carbon black cement composite for traffic monitoring *Constr. Build. Mater.* **154** 1079–86

[25] Cao J and Chung D 2004 Electric polarization and depolarization in cement-based materials, studied by apparent electrical resistance measurement *Cement Concr. Res.* **34** 481–5

[26] Downey A, D'Alessandro A, Ubertini F, Laflamme S and Geiger R 2017 Biphasic DC measurement approach for enhanced measurement stability and multi-channel sampling of self-sensing multi-functional structural materials doped with carbon-based additives *Smart Mater. Struct.* **26** 065008

[27] Vertuccio L, Vittoria V, Guadagno L and Santis F D 2015 Strain and damage monitoring in carbon-nanotube-based composite under cyclic strain *Composites* A **71** 9–16

[28] Wang S and Chung D 2006 Self-sensing of flexural strain and damage in carbon fiber polymer-matrix composite by electrical resistance measurement *Carbon* **44** 2739–51

[29] Downey A, Garcia-Macias E, D'Alessandro A, Laflamme S, Castro-Triguero R and Ubertini F 2017 Continuous and embedded solutions for SHM of concrete structures using changing electrical potential in self-sensing cement-based composites *Nondestructive Characterization, Monitoring of Advanced Materials, Aerospace and Civil Infrastructure 2017* ed H F Wu *et al* (Bellingham, WA: SPIE)

[30] Downey A, D'Alessandro A, Baquera M, García-Macías E, Rolfes D, Ubertini F, Laflamme S and Castro-Triguero R 2017 Damage detection, localization and quantification in conductive smart concrete structures using a resistor mesh model *Eng. Struct.* **148** 924–35

[31] Doltsinis I and Kang Z 2004 Robust design of structures using optimization methods *Comput. Methods Appl. Mech. Eng.* **193** 2221–37

[32] Downey A, Hu C and Laflamme S 2017 Optimal sensor placement within a hybrid dense sensor network using an adaptive genetic algorithm with learning gene pool *Struct. Health Monit.* 147592171770253

[33] Wong I, Loh K J, Wu R and Garg N 2015 Effects of ultra-low concentrations of carbon nanotubes on the electromechanical properties of cement paste *Nanotechnology in Construction* (Berlin: Springer) pp 371–6

[34] Vogt H and Nenzi P 2014 *Ngspice Users Manual—Version 26*

[35] Han B, Guan X and Ou J 2007 Electrode design, measuring method and data acquisition system of carbon fiber cement paste piezoresistive sensors *Sens. Actuators* A **135** 360–9

[36] Janesch J 2013 Two-wire versus four-wire resistance measurements: which configuration makes sense for your application? *Technical Report* Keithley Instruments